Water-Dispersible, Ligand-Free, and Extra-Small (<10 nm) Titania Nanoparticles: Control Over Primary, Secondary, and Tertiary Agglomeration Through a Modified "Non-Aqueous" Route

Christopher J. Cadman, Andrea Pucci, Francesco Cellesi, and Nicola Tirelli**

1. Introduction

The attractive photochemical/photophysical properties of titanium dioxide-based materials include the efficient photo-induced generation of oxidants/free radicals (reactive oxygen species, ROS) at surface sites and have made them popular for use in applications such as photovoltaics,[1] gas sensing,[2] surface (window) self-cleaning,[3] sun protec-tion,[4] water purifi cation,[5] and so forth.

TiO_2 is also commonly employed in biomaterials. For example, titania-coated materials are known to be beneficial for osteointegration,[6] although with a strong dependency on the surface morphology[7] and possibly because of a mechanism of protein adsorption similar to hydroxyapa-tite.[8] Additionally, titania nanoparticles show a relatively low acute toxicity ¦[9] above all in comparison to other inor-ganic nanoparticles;[10,11] however, they can also cause oxidative stress under photoactivation, resulting in infl amma-tory reactions[12] and damage to nucleic acids[13] and to cell membranes,[11] with detrimental effects on cell viability; inter-estingly, this behavior appears to be more noticeable on tumoral cells.[14]

As suggested since the '90s, the (photo) oxidative activity of titania nanoparticles

may be employed to produce cytotoxic ROS as a therapeutic tool,[15] by targeting their photo-genera-tion to selectively irradiated cells/cell masses; this approach is essentially identical to photodynamic therapies based on low molecular weight sensitizers, for example, porphyrins and phtalocyanins.[16,17]

Received: June 11, 2013
Revised: July 22, 2013
Published online: October 8, 2013

Dr. C. J. Cadman
Manchester Pharmacy School
UniversityofManchester
OxfordRoad , Manchester, M139PT , UK
Dr. A. Pucci
Department of Chemistry and Industrial Chemistry
University of Pisa
via Risorgimento 35, 56126, Pisa, Italy
Dr. F. Cellesi
CEN – European Centre for Nanomedicine
PiazzaLeonardodaVinci32 , 20133, Milan, Italy
E-mail: francesco.cellesi@policlinico.mi.it
Dr. F. Cellesi
Fondazione IRCCS Ca' Granda
Ospedale Maggiore Policlinico
ViaPace9 , I-20122, Milan, Italy
Dr. F. Cellesi
Department of Chemistry
Materials and Chemical Engineering "Giulio Natta,"
Politecnico di Milano
ViaLuigiMancinelli7 , 20131, Milano, Italy
Prof.N.Tirelli
Institute of Inflammation and Repair, and School of Materials
University of Manchester
Oxford Road, Manchester, M13 9PT, UK
E-mail:Nicola.tirelli@manchester .ac.uk

In view of such an application, the synthesis of titania nanoparticles should allow to exert control over the following variables:

a) crystalline phase: the combination of anatase and rutile has been shown to be more active than the isolated components[18]and indeed commercially available photocatalysts such as Degussa P-25 have a anatase/rutile 3:1 composition.[19] However, anatase is generally reported to be more active than rutile,[20] and the differences with mixed-phase photocatalysts can be easily offset by acting on other factors such as size and availability of surface sites.[21] Therefore, for seek of simplicity and ease of characterization, preparative methods yielding anatase are probably to favor.
b) surface chemistry: it is well known that surface modification with chromophoric groups, for example, with carotenoids[22] or dyes such as alizarin blue,[23] allows to extend the sensitivity of the photocalytic activity towards the visible region of the spectrum (essentially the same as for dye-sensitized solar cells), which would also allow deeper penetration of the radiation in biological tissues. Additionally, surface functionalization can allow to overcome agglomeration in water, due to the isoelectric point of titania (any crystalline form) being too close to neutrality to allow sufficient electrostatic stabilization.[24] Last, the introduction of appropriate surface groups (for example poly(ethylene glycol) (PEG) chains or peptide/proteic groups) is a prerequisite to minimize protein adsorption and allow both a prolonged circulation in body fluids and biological targeting. Ideally, synthetic procedures should therefore easily allow different forms of surface functionalization, and possibly to accomplish them in a water environment.
c) size: the photocatalytic activity of TiO_2 is directly proportional to the number of free surface sites available, therefore nanoparticles show higher photocatalytic activity than bulk TiO_2,[25] and smaller particles have a higher efficiency in ROS generation and phototoxicity than larger ones.[26] Additionally, the size of titania particles affects their biodistribution[9] and smaller particles are likely to diffuse faster in interstitial fluids allowing a more homogeneous distribution in a tissue. Ideally, in order to allow also blood-born applications, these particles should show the minimal size necessary to avoid renal filtration, which is in the range of 5–10 nm.

In order to extend the spectrum of nanoparticles employable for photodynamic therapy, in this study, we have specifically tackled the minimization of the size of water-dispersible titania nanoparticles; only a limited number of reports exist for the preparation of very small (10–20 nm) titania nanoparticles,[27,28] and in no case they have been studied in colloidal dispersion, possibly because of significant agglomeration during their preparation.

Classical preparative techniques have been based on aqueous sol–gel and hydrothermal methods,[29] but more recently non-aqueous sol–gel synthetic routes have become more popular.[30–32] Due to the relatively slow condensation rate between surface groups, such methods offer a better control over average size, crystallinity, and surface composition;[33] for example, in aqueous sol–gel processes, the particle size can be controlled only through the use of relatively large quantities of surfactant,[34] which imposes strong limitations on the surface composition, while crystallinity is induced only a posteriori via calcination.[28] Reviews from Niederberger provide an in-depth overview on the advantages of non-aqueous sol–gel methods for the production of metal oxide nanoparticles.[33,35]

In a previous paper, we have employed a non-aqueous process in benzyl alcohol, where $TiCl_4$ and ethanol in situ produce $Ti(Cl)_{4-n}(OEt)_n$ (n close to four), whose thermal condensation at 80 °C eventually produced anatase nanoparticles with a virtually ligand-free surface and an average diameter in the region of 30 nm.[36] The nanoparticles can then be easily functionalized, for example, with catechols, possibly bearing also PEG chains.[37] In addition to the typical advantages of non-aqueous processes, this "benzyl alcohol method"[38] allows the preparation of ligand-free nanoparticle dispersions in acidic water, due to the contemporaneous and rapid occurrence of the hydrolysis of alkoxide surface groups and of the surface protonation, which allows electrostatic stabilization. It is also worth mentioning that the use of the toxicologically benign benzyl alcohol as a solvent is an additional advantage in the perspective of a medical use.[39] However, despite the significant advantages of the benzyl alcohol method (chiefly the control over size and surface chemistry), the mechanism of nanoparticle formation and growth is yet rather poorly understood; in particular, a generally unexplained lag time is often observed prior to the appearance of primary crystalline particles.[40]

Here, we have worked on the hypothesis that traces of water may strongly influence both the nature of the growth mechanism and the presence of the lag time; we have therefore modified the synthetic approach so as to enable a higher degree of control over the different phases of growth. In our synthesis, the poorly defined starting material has been replaced by $Ti(OR)_4$ where R is either a propyl ($Ti(OPr)_4$), butyl ($Ti(O\mathit{n}Bu)_4$), or isopropyl ($Ti(O^i\mathit{n}Pr)_4$) group, and we independently varied the amounts of HCl (as both a catalyst for condensation reactions and a protonating agent for colloidal surfaces) and water. The titanium alkoxides were chosen to guarantee a clear initial stoichiometry to the titanium centers and to understand the effect of the nature of alkoxy groups on the rate of particle growth. Water was added to clarify the possibility of its direct role in the nucleation of primary particles (**Scheme 1**). We have then focused on the characterization of the successive phase of thermal growth, which can in principle be based on the agglomeration of primary particles (and condensation of surface groups, producing ethers or alcohols) or on their growth via the condensation of additional titanium alkoxides. Last, we have also studied the conditions leading to the minimization of nanoparticle agglomeration during the final re-dispersion in water and their dependency on the nature of the organic residues of the titanium alkoxides.

2. Results and Discussion

2.1. Role of Water in the Non-Aqueous Route

Despite being in principle a non-aqueous process, the "benzyl alcohol route" can be significantly influenced by the presence

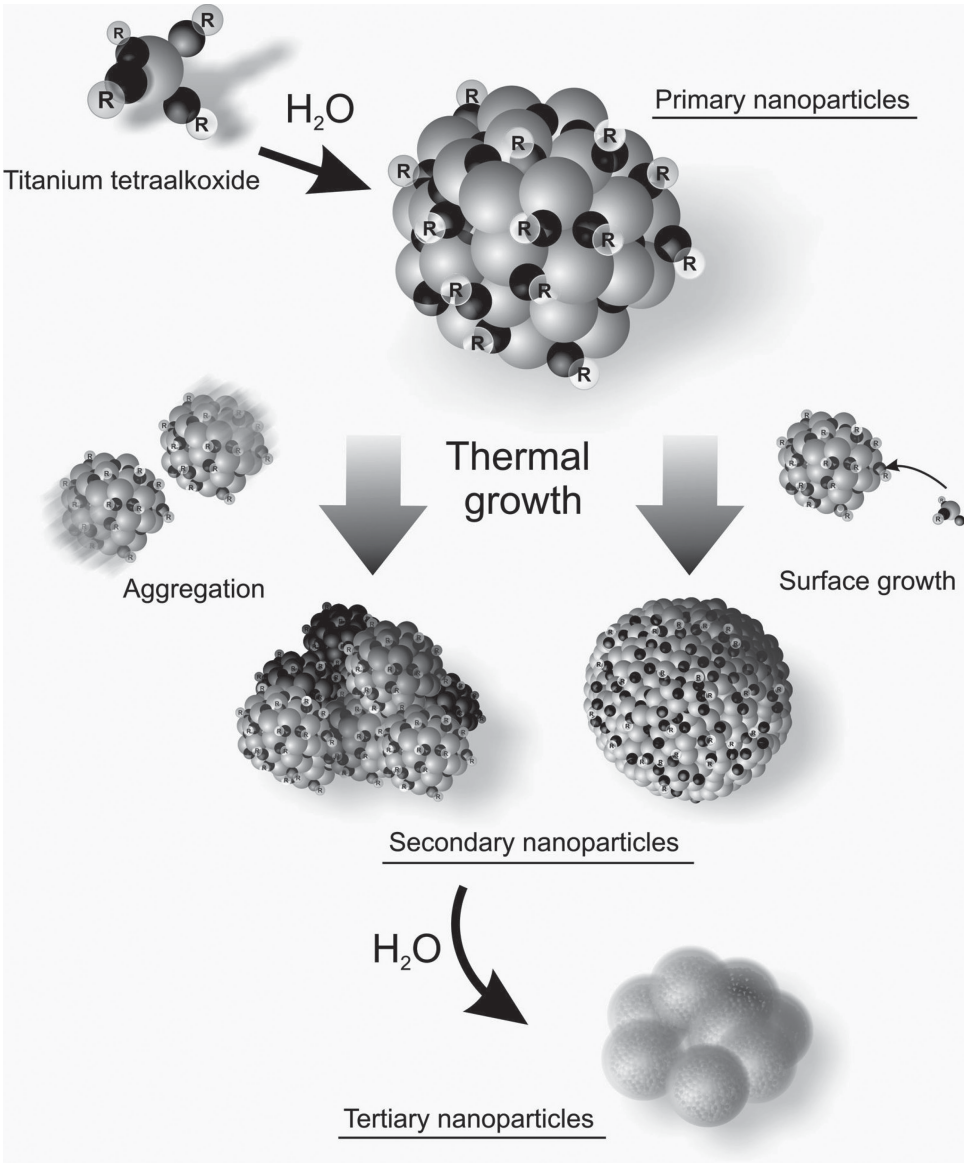

Scheme 1. Primary TiO_2 nanoparticles are instantly formed upon the addition of H_2O to the titanium alkoxide precursor. Subsequent heating causes growth of these particles into larger colloidal objects, which may be produced from primary particles via their aggregation or through the condensation of monomeric titanium species on their surfaces. In both cases, the growth phase will require the presence of condensation reactions, which may release alcohols or ethers as leaving groups. In the case of growth via aggregation, one can obtain more or less compact aggregates depending on the ease of the collision between particles; a decreasing compactness is numerically expressed as an increasing fractal dimension. Finally, the dispersion of secondary particles in a water environment will cause hydrolysis of the residual alkoxy surface groups and possibly additional agglomeration to yield tertiary nanoparticles.

of water. We have initially noticed this phenomenon by using the reaction of ethanol and $TiCl_4$ in benzyl alcohol to produce anatase nanoparticles[36,37] (**Figure 1**; preparation described in Supporting Information, Section 1): in a humid environment (moist argon bubbled in the reaction environment), nanoparticles can be detected relatively quickly and rapidly grow in size, while decreasing the humidity they present a much slower growth (flow of dry argon, reactor open) or can also not condense at all (no evidence of nanoparticles after up 10 h using dry argon and sealed reactors). This effect of water may go unnoticed because most commonly the synthesis of metal oxides via the benzyl alcohol route is performed under air and with non-anhydrous benzyl alcohol, therefore traces of water can easily be present.

The accelerating effect of water could be ascribed to two possible phenomena:

a) the direct involvement of water. In the benzyl alcohol route this may correspond to the hydrolysis of Ti–Cl bonds or of in situ formed titanium alkoxides, to eventually produce titanols, which have always been considered the most reactive groups in the production of Ti–O–Ti groups.[41] This would

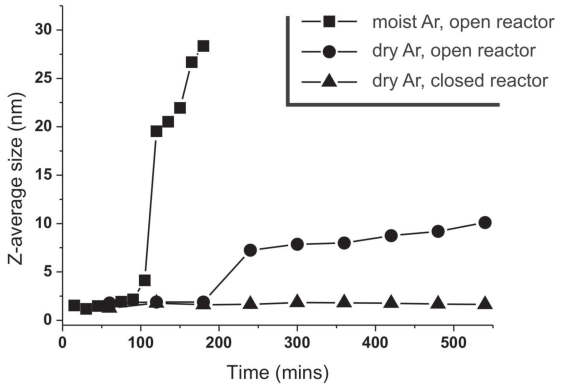

Figure 1. Evolution of nanoparticle size in tbe reaction between $TiCl_4$ and ethanol (1:10 molar ratio) in benzyl alcohol at 80 °C (see Supporting Information for the preparative details). Under completely inert conditions no nanoparticles were formed, however, whilst leaving the reaction open nanoparticles form after an initial lag time of around 3 h. Whilst performing the reaction under a H_2O saturated atmosphere nanoparticles were formed after a short lag time of 90 min, then growing in an uncontrollable fashion.

not contradict the occurrence of non-titanol based reactions, which have been demonstrated in the benzyl alcohol route (elimination of ethers or halides)[42,43] but would suggest that they may be operating as secondary condensation mechanisms.

b) a hydration-dependent catalytic activity of the HCl (more or less "naked" H^+).

2.2. Primary Particles (Room Temp. Nucleation)

In order to clarify the role of water, we have tried to separate the preparative variables modifying the classical benzyl alcohol route by 1) adding HCl to preformed titanium alkoxides instead of producing them in situ through the reaction of $TiCl_4$ + alcohols, for a better control over pH; 2) using a series of alkoxides with variable hydrophobicity and resistance to hydrolysis ($Ti(OnPr)_4$, $Ti(O^iPr)_4$, $Ti(OnBu)_4$; $Ti(OEt)_4$ was excluded due to its too rapid reactivity) as the means to identify effects due to the aliphatic groups (if there are, there must be a variation of properties in the series); it is noteworthy that the bulkiness of the alkyl residues should also allow to reduce the exchange with benzyl alcohol.

The size of the colloidal products of this early phase of condensation was used as a measure of the effects of the nature of the alkoxide, of acidity (expressed through the Cl/Ti molar ratio) and of the water content (expressed through the H_2O/Ti molar ratio). We have first focused on the particles produced upon mixing of the reagents at room temperature, which were typically sized 2.5–5 nm and are hereafter referred to as primary nanoparticles.

Negligible differences were recorded among the three alkoxides. For all of them, and independently on the HCl content, the nanoparticle size increased with increasing water content, with the limit of macroscopic precipitation for H_2O/Ti>4 (**Figure 2**, left and center). Interestingly, this ratio is close to the theoretical complete conversion of alkoxide to titanols, therefore it is reasonable to assume that macroscopic aggregation occurs upon quantitative hydrolysis.

The lack of differences imputable to the alkoxides and the predominant role of water suggest that a) primary nanoparticles are formed through titanol condensation, while direct titanol condensation would appear to have a negligible role under these conditions (room temperature and acidic environment), b) their surface should present an alkoxide-rich surface, acting as a barrier towards further aggregation. It is noteworthy that at H_2O/Ti = 4 a significant amount of alkoxides must still present, therefore the surface of primary nanoparticles is likely to present also mixtures of alkoxides and titanols.

HCl concentration seemed to have an effect on primary particle size only for Cl/Ti ≤ 0.5 (Figure 2, right), under which conditions the presence of macroscopic aggregates became appreciable; since the formation of chlorinated species would determine an opposite trend (higher reactivity and thus larger size with increasing Cl content), we are inclined to ascribe this effect to a lack of electrostatic stabilization due to insufficient surface protonation.

2.3. Secondary Particles (Thermal Growth)

Primary nanoparticles were indefinitely stable at room temperature but, as for the classical non-aqueous route, it was possible to increase their size upon heating. This growth is attributable

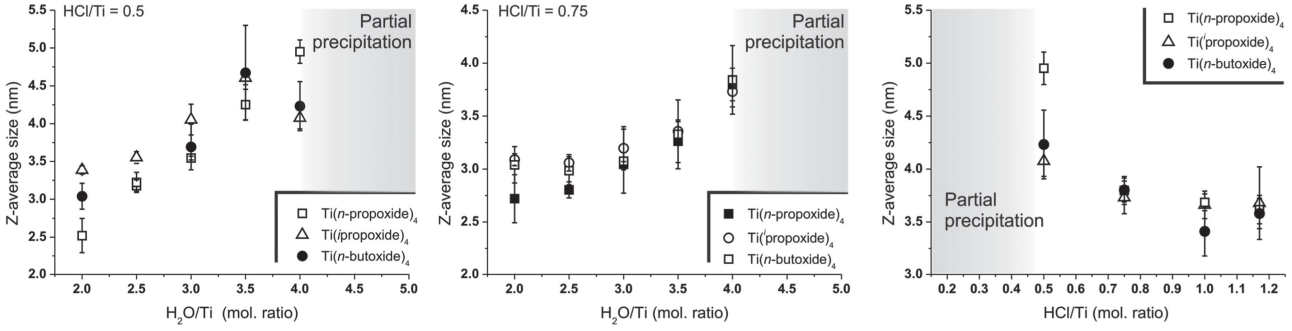

Figure 2. Left and center: Size of primary nanoparticles as a function of the water content at a constant HCl concentration (Cl/Ti mol. ratio = 0.75 in the left graph and = 0.5 in centre graph). In all experiments [Ti] = 456 mM. Right: Size of primary nanoparticles as a function of HCl concentration at a constant water content (H_2O/Ti mol. ratio = 4). Error bars are calculated on the basis of three separate preparative experiments.

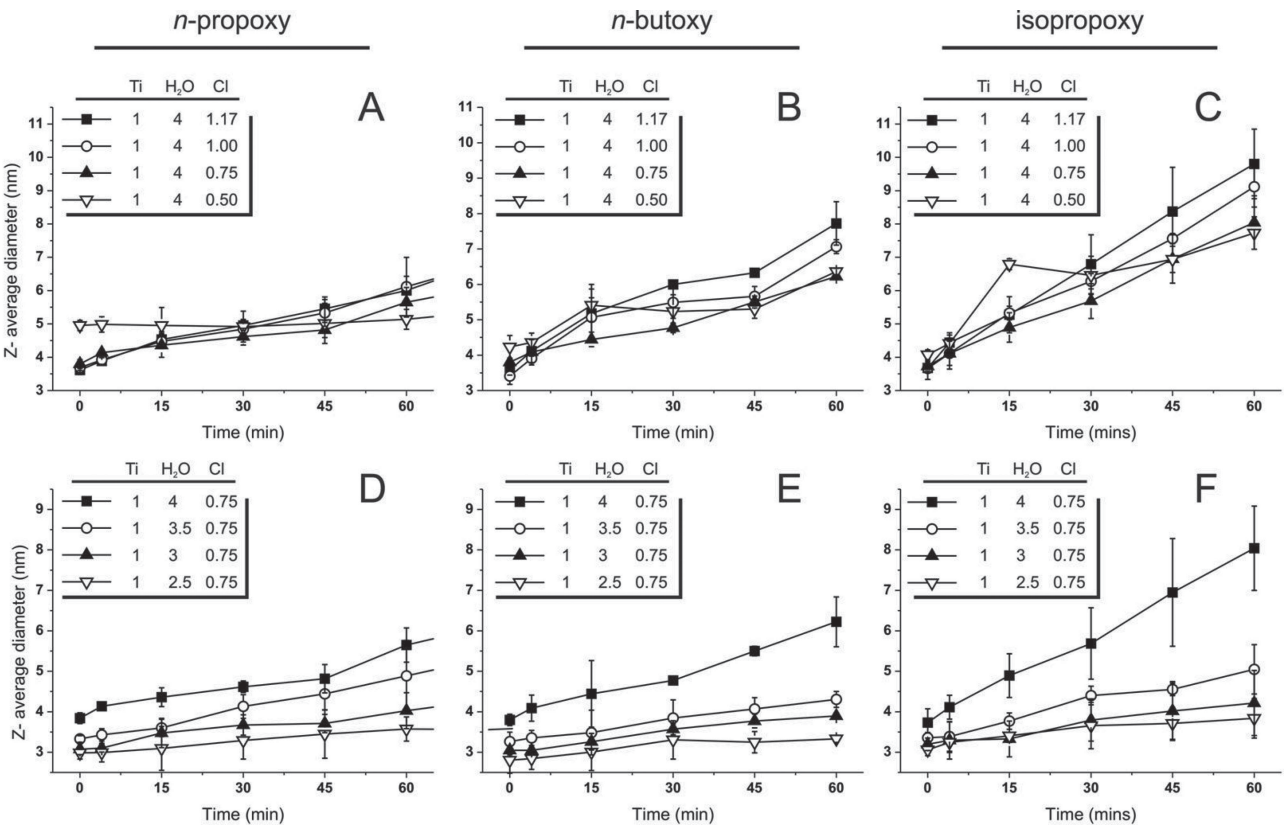

Figure 3. Evolution of size (DLS measurements, T = 80 °C) as a function of time and of the amount of A–C) HCl or of D–F) water added to solutions of Ti(O*n*Pr)$_4$ (left),Ti(O*n*Bu)$_4$ (center), and Ti(O^{i}Pr)$_4$ (right). Error bars are calculated on the basis of three separate preparative experiments.

to further condensation of surface alkoxide groups either between themselves (aggregation of primary particles) or with monomeric titanium alkoxides (growth via surface condensation on primary nanoparticles) to yield larger colloidal objects, which are hereafter termed secondary nanoparticles. It is noteworthy that the mechanism of growth via aggregation would allow to explain the typical conglomerate morphology of the products of the classical non-aqueous process, where primary particles can still be recognized.[36]

In this thermal growth phase, the agglomeration kinetics showed a small accelerating effect of HCl concentration (**Figure 3**A–C, shown for H_2O/Ti = 4), which may be ascribed to its role as a catalyst in the process. However, differences in the internal structure of the final particles cannot be ruled out: a higher surface protonation could lead to a less compact aggregate due to repulsion between neighboring groups, and this would be reflected by a lower fractal dimension of the particles.

In terms of the titanium/water molar ratio, two different regimes are recognizable: A) primary particles prepared with H_2O/Ti< 4; the aggregation rate appeared to slightly increase with increasing initial amount of water; on the other hand, although butoxide-covered nanoparticles appeared to grow slower, the effects of the aliphatic residues were not statistically relevant(Figure 3D–F). B) Primary particles prepared with H_2O/Ti = 4; the growth kinetics was much more rapid and clearly alkoxide-sensitive (O^{i}Pr>>O*n*Bu≥O*n*Pr). The HCl concentation did not significantly influence the dependency on the water content; although more noisy due to their border-line stability, a similar trend was observed also for particles prepared with Cl/Ti = 0.5 (see Supporting Information, Figure 2SI). This accelerated growth under conditions where the presence of intact titanium tetraalkoxides is unlikely (H_2O/Ti = 4) would support the hypothesis of growth via aggregation, which is further confirmed by the increase in the width of the size distribution during the thermal treatment (see Supporting Information, Section 2 and Figure 3SI).

The surface of primary nanoparticles may present a significant amount of titanols; therefore, the growth by aggregation could be associated to the production of ethers (condensation of two alkoxides) or alcohols (titanol+ alkoxide condensation). A growth mechanism predominantly based on the formation of alcohols would explain the much slower growth under conditions that likely minimize the amount of titanols, that is, for H_2O/Ti< 4 and would also provide an easy explanation of the enhanced reactivity of isopropoxide-containing particles at H_2O/Ti = 4. Isopropanol boiling point (82 °C) is indeed very close to the reaction temperature, while the other alcohols are much less volatile (T_b = 98 and 118 °C, resp. for *n*PrOH and *n*BuOH) and would explain the similarly slower kinetics of the corresponding particles. This explanation would not hold for ethers as leaving groups: Ti(O*n*Pr)$_4$-derived particles do not grow much faster than Ti(O*n*Bu)$_4$-derived ones, although the corresponding ethers have very different boiling points (T_b = 90 vs 142 °C). However, it is worth pointing out that the

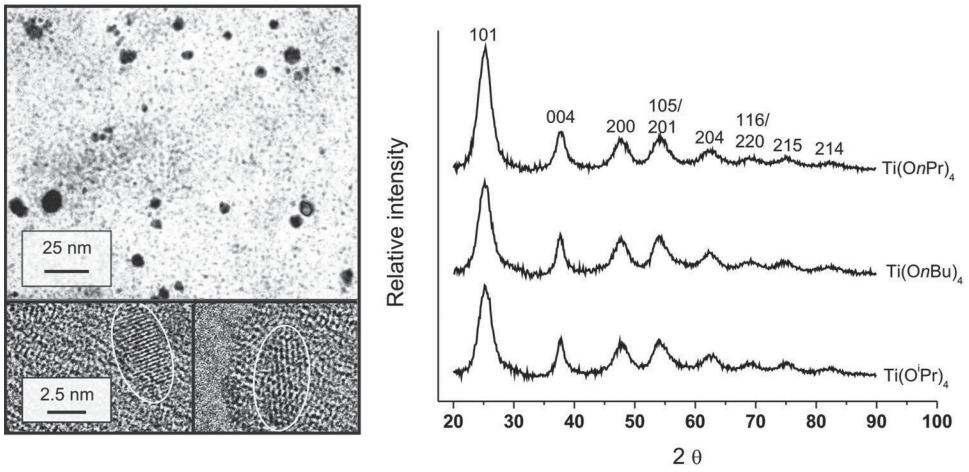

Figure 4. Left: TEM images of nanoparticles obtained from $Ti(O^iPr)_4$ in benzyl alcohol, $Ti:H_2O:HCl$ = 1:4:1.17. Most nanoparticles appeared to be sized in the region of 6–9 nm. High resolution images (bottom) show a 3.2 Å spacing between crystalline planes, which corresponds to the 101 crystal plane of anatase. Right: XRD patterns of nanoparticles freeze dried from an aqueous suspension prepared using the three different titanium tetraalkoxy precursors.

accelerated growth of $Ti(O^iPr)_4$-derived particles may also derive from a lower surface protonation of the very hydrophobic isopropoxy groups.

TEM broadly confirmed the dimensional data obtained via DLS (**Figure 4**, left) and it further showed the nanoparticles to be highly crystalline with 3.2 Å-spaced lattice fringes (Figure 3, right); this feature has already been recorded in the classical non-aqueous process[44] and corresponds to the spacing between the 101 planes of anatase.[45] XRD confirmed all nanoparticles to be essentially composed of highly crystalline anatase (**Table 1**), as for the classical non-aqueous process,[46] with an average crystallite size (different from particle size, which refers to the size of the actual colloidal particle, generally consisting of multiple crystallites) always in the range of 3–4 nm. This value is in good agreement with previous results of the classical non-aqueous route,[36] and strikingly corresponding to the size of primary nanoparticles, despite the approximations intrinsic to the Scherrer equation (e.g., that of a spherical shape of the particles).

It is also worth noting that a) the amount of acid catalyst did not appreciably influence either parameter, confirming its non-critical role in the process; b) the nature of the alkoxide appeared to have some effect on crystallinity, with a slight decrease in the order $O^iPr > OnPr \geq OnBu$ that may be a result of a different kinetics of primary particle formation.

Since primary particles can still be identified after the thermal growth phase, it can be concluded that secondary particles are likely formed through aggregation rather than surface growth of primary ones. Correspondingly, it can be expected the fractal dimension of the secondary particles to be <3, due to the statistical nature of the aggregation process. Typically, in a 3D structure, the fractal dimension (D_f) would approach the value of 3 in the limit of very dense packing, while a dendritic structure can push this parameter significantly below 2.

Static light scattering (SLS) is the most commonly used method for the determination of the fractal dimensions of colloids:[50–52] by plotting the scattered intensity I as a function of the scattering vector $q = \frac{4\pi n \sin\vartheta}{\lambda}$ in a log–log plot, it is generally possible to calculate the D_f of aggregates as the slope of the graphs. The main underlying assumption is that the dependency of I on q is mostly due to the structure factor $S(q)$, which scales with q as a power of D_f, that is, $S(q) \propto q^{-D_f}$; this assumption, however, is valid only when the aggregated particles have an average radius of gyration comparable or larger than the wavelength of the light used in the experiments (specifically, it should be $<R_g> \gg q \gg 1$). This condition is not fulfilled in the present case; for example, at the end of the growth phase the largest nanoparticles, that is, $Ti(O^iPr)_4$-derived nanoparticles produced with 1 : 4 : 1.17$Ti\text{-}H_2O$:HCl molar ratio, showed $<R_g> \approx$ 16 nm (see Supporting Information, Figure 3SI), which is far too small in comparison to the wavelength of visible light. Correspondingly, log(I) versus log(q) plots do not provide useful information about D_f (see Supplementary Information, Figure 3SI). An alternative SLS approach would use the relationship between $I(0)$ (intensity at $q = 0$) and the $\frac{<R_g>}{R_p}$ ratio (R_p being the radius of the primary

Table 1. Anatase content and crystallite size of nanoparticles as a function of the amount of HCl and of the nature of the titanium alkoxide.

$Ti:H_2O$:HCl molar ratio	Crystallite size [nm][a]			Anatase content [wt%][b]		
	$Ti(OnPr)_4$	$Ti(OnBu)_4$	$Ti(O^iPr)_4$	$Ti(OnPr)_4$	$Ti(OnBu)_4$	$Ti(O^iPr)_4$
1 : 4 : 1.17	3.9	3.7	4.1	83	80	98
1 : 4 : 1	4.1	3.9	4.1	96	82	95
1 : 4 : 0.75	4.0	3.9	4.0	91	84	97
1 : 4 : 0.50	4.0	3.5	3.6	86	84	90

[a]The crystallite size was calculated through the Scherrer analysis[47] of the 101 peak; the data may not precisely estimate the actual crystallite size and methods other than Scherrer's ones can be used in alternative;[48]; [b]Calculated from the area of 101 peak,[49] as described in the Experimental Section.

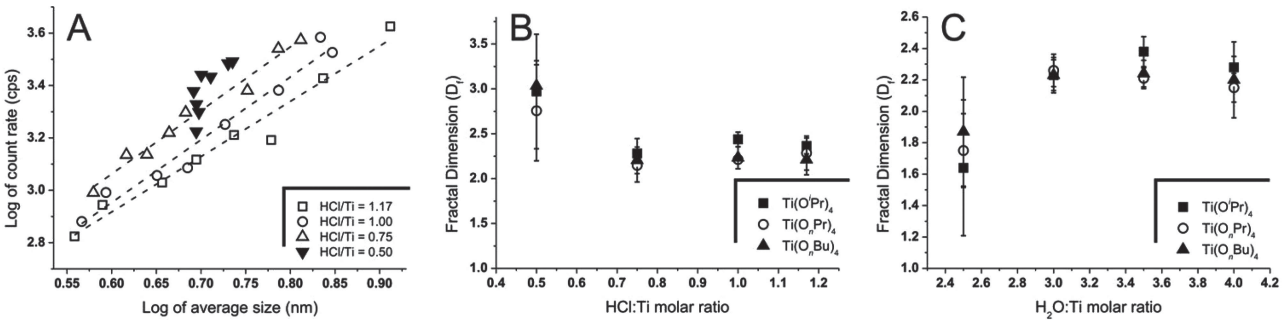

Figure 5. A) Log–log plot of nanoparticle Z-average size versus equivalent count rate at different times for (precursor: $Ti(O^iPr)_4$; $Ti:H_2O$ = 1:4); the dashed lines show the results of fittings. Please note that in this series of data, the slope at Ti:HCl = 0.5:1 D_f is basically undefined. B) Dependency of the fractal dimension of secondary nanoparticles on the acid content for $Ti:H_2O$ = 1:4. C) Dependency of the fractal dimension of secondary nanoparticles on the amount of water used in primary particle nucleation (Ti: HCl = 1:4).

particles), whose slope in a log–log plot would again provide the fractal dimension.[53,54] However, this approach is rather cumbersome (a Zimm plot per time point) and is affected by significant errors in the estimation of $<R_g>$ at early time points, due to the contribution of primary particles. A considerably simpler approach has been employed on similarly sized titania nanoparticles (5–40 nm) by the group of Kanaev, who have used the relationship between log(I) and log(R_H) to calculate D_f as the slope of the corresponding log–log graphs (**Figure 5**A).[55] The theoretical foundation of this simplified method is essentially the same as for obscuration method proposed by Wu and Morbidelli (scattered intensity $\propto (\frac{<R_g>}{R_p})^{Df}$), but the approximation of the particle dimension with the hydrodynamic radius is advantageous since it allows measurements to be performed in DLS mode (i.e., single angle, single concentration), although with a likely reduction in precision. We have accordingly fitted the scattering data recorded during the thermal growth phase, obtaining fractal dimensions always <3 (Figure 5B,C).

It is noteworthy that rather high values of fractal dimension (2.2–2.4) were observed for most conditions; these figures are typical for aggregates produced by particles with slow aggregation kinetics due to the presence of a repulsion barrier, which in our case is of electrostatic nature (protonation);[56] however, we cannot exclude a compaction of the cluster during the thermal phase, possibly due to the occurrence of additional, intra-cluster condensation reactions. The values obtained at low water/Ti and Cl/Ti ratios present high variability and should not be considered as statistically relevant; see, for example, the data points for Cl/Ti = 0.5 in Figure 5A, where the fractal dimension almost diverges due to the presence of large aggregates. A final indication of the production of secondary particles through agglomeration comes from the comparative analysis of radius of gyration and hydrodynamic radius: at the end of the thermal growth phase $<R_g>/<R_H>$ = 1.5 – 2 (see later in **Table 2**). Such values are typically assumed to be an indication of irregular morphology obtained through statistical (and reaction-limited) agglomeration as opposed to a spherical one for which $<R_g>/<R_H><1$.[57] High $<R_g>/<R_H>$ ratios can sometimes be also an indication of a broad size distribution, but this does not appear to be the case (all distributions with a width at half height of about 15 nm).

2.4. Tertiary Particles (Solvent-Dependent Agglomeration)

In this part of the study, we have employed secondary nanoparticles produced from the three titatnium alkoxides with a $Ti:H_2O:HCl$-1:4:1.17 molar ratio (maximization of stability and thermal growth kinetics) and a size peaked around 7.5 nm. The particles can be precipitated via addition of diethyl ether and then easily redispersed in benzyl alcohol, without any change in their size distribution (**Figure 6**, top); this indicates that no significant aggregation occurred in the precipitate.

Similarly to what was previously seen for larger titania nanocrystals,[36] the particles can also be precipitated and then redispersed in acid water (pH = 2), which allows at the same time full hydrolysis of the residual surface alkoxides and electrostatic stabilization due to protonation. However, in water the nanoparticles showed a titanium alkoxide-dependent variation in their size, with O*n*Pr>O*n*Bu>O^{i}Pr. (Figure 6, bottom).

Table 2. Mass loss associated to evaporation of water and elimination of other volatile products for nanoparticles prepared with a $Ti:H_2O:HCl$ 1:4:1.17 molar ratio.

Precursor →	$Ti(n\text{OPr})_4$		$Ti(\text{O}n\text{Bu})_4$		$Ti(O^iPr)_4$	
	before H_2O	after H_2O	before H_2O	after H_2O	before H_2O	after H_2O
$<R_g>/<R_H>$	1.5 ± 0.3	3.3 ± 0.1	1.9 ± 0.8	3.8 ± 0.1	2.2 ± 0.3	3.8 ± 0.1
Mass loss [wt%]						
"free" H_2O[a)]	13.4	10.7	17.4	13.8	14.6	14.6
bound H_2O, TiOR/OH [b)]	18.4	6.1	21.6	6.2	21.6	6.9

[a)]Calculated from the relative mass loss after an isothermal treatment at 120 °C; [b)]Calculated from the relative mass loss at 500 °C in relation to the "dry" weight of the nanoparticles, i.e., considering the weight at 125 °C as 100%.

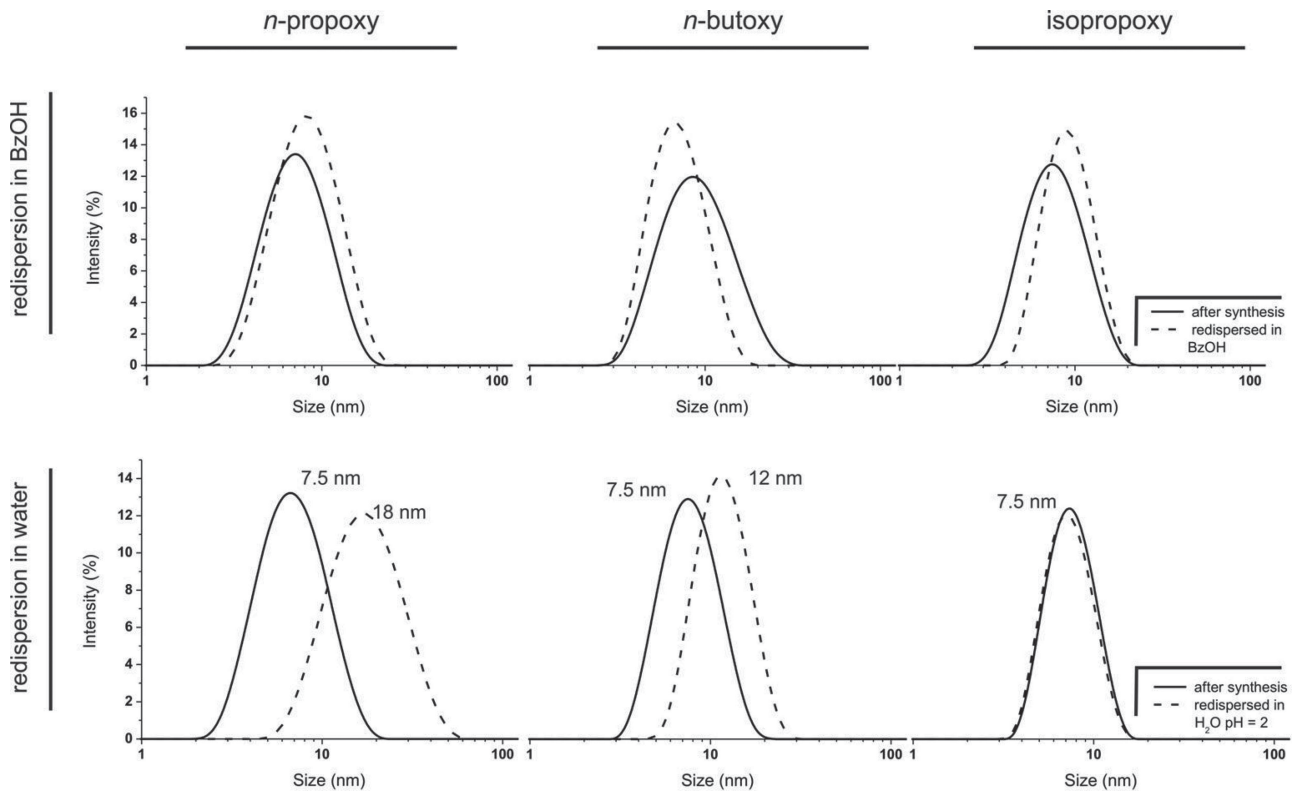

Figure 6. Size distribution of nanoparticles prepared from Ti(O*n*Pr)$_4$ (left), Ti(O*n*Bu)$_4$ (center) and Ti(O^{i}Pr)$_4$ (right) in benzyl alcohol at $H_2O/Ti = 4$; the particles were heated at 80 °C for the time necessary to reach an identical final size (= degree of agglomeration) of 7.5 nm. The nanoparticles were precipitated in diethyl ether and redispersed in benzyl alcohol (top) or in water at pH = 2 (bottom). The process of redispersion in water induced a variable degree of aggregation, which appears to correlate inversely to the hydrophobicity of the aliphatic residues; this effect was quantitatively reproducible (at least three separate experiments with negligible differences in *Z*-average size and width of the distribution). Nanoparticle concentration: 10 mg mL^{-1} after redispersion.

The $<R_g>/<R_H>$ was similar for all particles and considerably larger than what recorded in benzyl alcohol (Table 2, first row), which is consistent with further agglomeration to produce more "dendritic" colloids, hereafter referred to as tertiary nanoparticles. It is noteworthy that the hydrodynamic size of particles prepared from Ti(O^{i}Pr)$_4$ was substantially unaltered, but their radius of gyration considerably increased (from 16.9 ± 1.9 to 28.4 ± 0.3 nm); therefore, it is likely that some form of further aggregation even with this alkoxide.

We want here to focus on the alkoxide-dependent difference in tertiary nanoparticle size, which can only be ascribed to the behavior of alkoxide-covered surfaces during water re-dispersion. IR spectra (**Figure 7**A) showed that organic species were present in the precipitate; they appeared also to include benzyl groups, which suggests a partial, although by far not quantitative exchange of the surface alkoxides. The organic species disappeared upon re-dispersion in water; in TGA the re-dispersion was accompanied by the substantial reduction of the high-temperature mass loss step, from ≈20 to ≈6 wt% of the dry mass (Figure 7B and Table 2).

It is noteworthy that OH groups were present both before and after re-dispersion in water; due to the characteristic δOH at 1600 cm^{-1} and the considerable mass loss upon 120 °C isotherm in TGA, it is possible to identify them as water in both cases, most likely adsorbed on the positively charged nanoparticles during isolation and analysis.

Since aggregation cannot be ascribed to phenomena occurring in the precipitate, it is reasonable to relate it to the different hydrolysis behavior of the surface alkoxides. However, rather unexpectedly the extent of aggregation appears to be inversely proportional to the hydrophobicity/bulkiness of the alkoxides, and thus also to their rate of hydrolysis. We interpret it as follows: we know that titanols promote aggregation, while positive charges discourage it; the slow reactivity of isopropoxy groups could allow dispersion of the precipitate and dense protonation of nanoparticles before significant hydrolysis has occurred; in this way, when titanol groups are introduced on diluted and highly charged particles, they would not have appreciable effect on their aggregation.

With an appropriate choice of the nature of the alkoxide residues it was therefore possible to control different stages of aggregation (thermal growth, water re-dispersion), ultimately allowing for a fine control over the size of water-dispersed ligand-free tertiary nanoparticles. This point has a profound influence on the final properties of the particles; for example, the nanoparticle size heavily affects their photocatalytic efficiency, which in this case was assessed

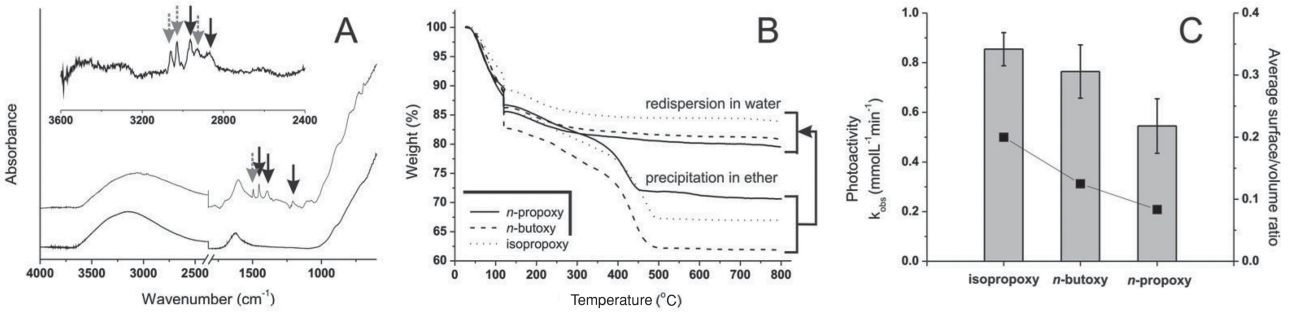

Figure 7. A) IR spectra of nanoparticles prepared from $Ti(O^iPr)_4$ with a $H_2O/Ti = 4$ molar ratio precipitated from diethyl ether (top) and after re-dispersion in acidic water and drying at 120 °C (bottom). The inset shows a magnified view of the 2400–3600 cm^{-1} region of the upper spectrum after baseline subtraction of the OH stretching band. Water is easily recognizable in both spectra from the presence of a broad OH stretching peak 2500–3500 cm^{-1} and from the OH bending one at 1600 cm^{-1}. The isopropyl groups can be recognized (black arrows) through the peaks at 2964 and 2875 cm^{-1} (resp. asymmetric and symmetric CH_3 stretching), by the sharp band at 1450 cm^{-1} and the broad one around 1390 cm^{-1} (resp. asymmetric CH_3 bending and most likely coalescence of the two bands associated to geminal symmetric CH_3 bending). Benzyl groups (grey arrows) can be recognized from the peaks 3028 and 3059 cm^{-1} (two forms of = C–H stretching), at 1495 cm^{-1} (aromatic ring breathing) and possibly at 2925 cm^{-1} (asymmetric CH_2 stretching). B) TGA runs of nanoparticles before and after redispersion. An isotherm was held at 120 °C until constant weight to ensure the full desorption of water, which was present in all samples as already appeared in infrared analysis. C) Pseudo-first-order rate constants for the methylene blue photodegradation reaction (grey bars) and average surface-to-volume ratios (black squares) for tertiary nanoparticles prepared from the three alkoxide precursors (H_2O/Ti = 4 molar ratio). Please note that the surface-to-volume is calculated assuming as calculated as $3/4\frac{1}{<R_H>}$ assuming a spherical geometry; this is a rather rough approximation, considering the likely heavily fractal nature (= low degree of compactness) of the particles. Nanoparticle concentration: 0.2 mg mL^{-1}, methylene blue: 0.025 mM.

using the photodegradation kinetics of a commonly used model choromophore, methylene blue. The pseudo-first-order degradation rate of methylene blue scaled well with the surface-to-volume ratio of the tertiary nanoparticles, (Figure 7C), therefore showing how the choice of the titanium alkoxide allows to control also the photoactivity of the final nanoparticles.

3. Conclusion

In this study we have successfully produced < 10 nm anatase nanoparticles fully dispersable in water, with high photocatalytic activity and a fully exchangeable surface. By doing this, we have also demonstrated a few key points of the non-aqueous route: a) the non-aqueous route to titanium dioxide could in reality be based on the presence of traces of water; the careful dosage of water (and HCl) allows not only to avoid the lag time typical of non-aqueous processes,[36,40,42] but also to operate a very precise control over dimensions and aggregation of primary titania nanoparticles; b) the process of thermal growth leading to secondary nanoparticles is due to the aggregation of primary ones and appears to be much dependent on the amount of OH groups present on their surface; this suggests the dominating reaction to be the elimination of alcohols rather than ethers. This reaction-limited aggregation has a statistical nature, leading to particles with a fractal structure (fractal dimension generally in the range 2.2–2.4); c) both thermal growth and re-dispersion in water are much influenced by the nature of the organic residues of the titanium alkoxides; in particular, in a counter-intuitive fashion the more hydrophobic isopropoxy residues appear to minimize aggregation during re-dispersion.

It is worth pointing out that b) broadly confirms what was observed by Jensen et al. in a system based on the in situ generation of titanium tetraethoxide from $TiCl_4$ and ethanol in benzyl alcohol: suddenly generated primary particles agglomerate in fractal and (in that case) anisotropic structures during thermal treatment.[40]

4. Experimental Section

Materials: Titanium (IV) tetrachloride ($TiCl_4$, purity 98%),, tetra *n*-propoxide ($Ti(OC_3H_7)_4$, purity 98%), titanium (IV) tetra *n*-butoxide ($Ti(OC_4H_9)_4$, purity ≥97.0%), titanium (IV) tetraisopropoxide ($Ti(OCH(CH_3)_2)_4$, purity ≥97.0%), benzyl alcohol (anhydrous, purity 99.8%), 37% hydrochloric acid solution, and 0.1 N hydrochloric acid solution were supplied by Sigma-Aldrich (Dorset, UK). Diethyl ether (anhydrous) was supplied by Fisher Scientific U.K. Ltd. All materials were used as received from the supplier without any further purification. Water was pre-deionised (Ellga) and further purified by a Milli-Q system (Millipore, U.K.)

Preparation of Nanoparticles: In each reactor of a Radleys Carousel 12 plus Reaction Station (Radleys, UK) $Ti(OR)_4$ (R = propyl, butyl, or isopropyl; 9.12 mmol) was added under argon to benzyl alcohol (20 mL) containing appropriate amounts of water and hydrochloric acid to provide $Ti:H_2O:Ti$ molar ratios of 1 : 4, 3.5, 3, 2.5: 0.75 (constant HCl concentration) or 1 : 4 : 1.17, 1, 0.75 (constant water concentration); the highest HCl concentration was obtained by directly adding 37% HCl to benzyl alcohol, while all other ratios were obtained by using appropriately diluted aqueous HCl. The pale yellow mixtures were vigorous stirred (magnetic agitation in 20 mL Carousel vials, 750 rpm) for 5 mins and the presence of dispersed objects was assessed via DLS; in control experiments the size of the dispersed objects was monitored for up to 24 h.

The reactions were then rapidly heated and reached the temperature of 80 °C at time = 4 min, when samples were taken, and then again every 15 mins until either the nanoparticles reached the size of 7–10 nm or no growth could be observed. The reactions were cooled to room

temperature, and in control experiments the size of the nanoparticles remained stable for at least 48 h.

The nanoparticle dispersions were then precipitated in diethyl ether (150 mL) and centrifuged (3500 rpm, 5 min). The supernatant was decanted and the resulting white solid was washed twice with 50 mL of diethyl ether. The precipitate was then re-dispersed in 50 wt%. water/ethanol solution at pH = 2 (obtained with 0.1 N HCl; 20 mL). The resulting solution was dialysed against purified water at pH = 2 using a regenerated cellulose dialysis membrane with a MWCO of 10 000 g mol^{-1}. The final concentration of the nanoparticle suspension (typically 10 mg mL^{-1}) was calculated by precipitating the content of 1 mL of sample by raising its pH using 1 N Na_2CO_3, followed by centrifugation (3500 rpm, 5 min) and decantation. The sample was washed with water and centrifuged again. 10 mL of water were finally added and the resulting suspension was freeze dried.

Photoreactivity of Nanoparticles: An Omnicure S1000 equipped with a 250–450 nm filter and an optical fibre with internal diameter of 5 mm (Omnicure liquid light guide) was used as a light source in all experiments; the output power at the end of the fibre was kept at 10 mW cm^{-2} and constantly monitored. The end of the fibre was vertically placed on a 25 mL two-neck round bottomed flask using a 10 cm-long glass tube as a connector; the entire assembly was covered with aluminium foil to avoid light dispersion. In a general procedure, 5 mL of methylene blue aqueous solutiona (8 μg mL^{-1} = 0.025 mM) containing titania nanoparticles (0.2 mg mL^{-1}; pH = 2 by HCl) were irradiated and the concentration of methylene blue was followed by continuously monitoring its absorbance at 665 nm (ε = 17,088 L mol^{-1} cm^{-1}) and fitting it with a pseudo first order model ($lnC(t) = -k_{obs}t + lnC_0$).

Physico-Chemical Characterization: Attenuated total reflection Infrared (ATR-IR) spectra were recorded in ATR mode ona Tensor 27 Bruker spectrometer. Dynamic light scattering (DLS) and ζ potential measurements were performed using a Zetasizer Nano ZS instrument (Malvern Instrument Ltd., UK) connected to a Malvern autotitrator MPT-2. Unless otherwise stated, quartz cuvettes with an optical path of 10 mm and disposable capillary flow cells were used respectively for DLS and ζ potential measurements. The calculation of the fractal dimension from DLS data was performed as described by Rivallin et al.[55] For thermogravimetric analysis (TGA),10 mg of freeze dried samples were analysed on a Mettler Toledo Starc System (TGA/SDTA851e) at a heating rate of 10 °C per minute under air; an isotherm at 120 °C was typically run until constant weight in order to ensure full water desorption. For transmission electron microscopy (TEM) analysis, (FEI Tecnai FEGTEM operated at 300 kV) 10 μL of a purified 1.7 × 10^{-4} mg mL^{-1} nanoparticle dispersion in acidic medium were pipetted onto a carbon coated 300 mesh grid. The dispersion was then freeze dried on the grid to avoid aggregation of the nanoparticles. X-Ray Diffraction (XRD) patterns were obtained in reflection mode with CuKα radiation on an IPD PW1800 diffractometer (PANalytical) using freeze dried nanoparticles. The diffractograms were recorded only on tertiary nanoparticles (after precipitation, redispersion in water and freeze drying). Primary nanoparticles were excluded: due to their small size, they could not be precipitated from benzyl alcohol and the direct drying of their dispersion may modify the particle morphology due to capillary forces. Further, tertiary nanoparticles were preferred to secondary ones, in order to eliminate any effect due to the surface alkyl groups. The fraction of crystalline (anatase) phase was calculated according to a literature method: considering W_A the anatase weight fraction, A_A the area of the anatase 101 peak and A_R the area of the 110 peak for a known amount of rutile standard added to the sample, and using a correction factor (0.884) calculated by Gribb and Banfield using known mixtures of finely crystalline anatase and rutile,[49] the weight fraction of anatase can be calculated as $W_A = \frac{0.884A_A}{0.884A_A + A_R}$. The Scherrer analysis allowed to estimate the size of crystallites in the agglomerated particles and was performed according to standard algorithms.[48]

Acknowledgements

C.J.C. gratefully acknowledges the Engineering and Physical Sciences Research Council (EPSRC) for funding his PhD studentship.

[1] M. K. Nazeeruddin, E. Baranoff, M. Gratzel, *Sol. Energy* **2011**, *85*, 1172.
[2] C. Mercado, Z. Seeley, A. Bandyopadhyay, S. Bose, J. L. McHale, *ACS Appl. Mater. Interfaces* **2011**, *3*, 2281.
[3] I. P. Parkin, R. G. Palgrave, *J. Mater. Chem.* **2005**, *15*, 1689.
[4] N. Serpone, D. Dondi, A. Albini, *Inorg. Chim. Acta* **2007**, *360*, 794.
[5] Q. L. Li, S. Mahendra, D. Y. Lyon, L. Brunet, M. V. Liga, D. Li, P. J. J. Alvarez, *Water Res.* **2008**, *42*, 4591.
[6] P. A. Ramires, A. Romito, F. Cosentino, E. Milella, *Biomaterials* **2001**, *22*, 1467.
[7] M. Bachle, R. J. Kohal, *Clin. Oral Implant. Res.* **2004**, *15*, 683.
[8] J. E. Ellingsen, *Biomaterials* **1991**, *12*, 593.
[9] J. X. Wang, G. Q. Zhou, C. Y. Chen, H. W. Yu, T. C. Wang, Y. M. Ma, G. Jia, Y. X. Gao, B. Li, J. Sun, Y. F. Li, F. Jiao, Y. L. Zhao, Z. F. Chai, *Toxicol. Lett.* **2007**, *168*, 176.
[10] T. J. Brunner, P. Wick, P. Manser, P. Spohn, R. N. Grass, L. K. Limbach, A. Bruinink, W. J. Stark, *Environ. Sci. Technol.* **2006**, *40*, 4374.
[11] C. M. Sayes, R. Wahi, P. A. Kurian, Y. P. Liu, J. L. West, K. D. Ausman, D. B. Warheit, V. L. Colvin, *Toxicol. Sci.* **2006**, *92*, 174.
[12] B. Trouiller, R. Reliene, A. Westbrook, P. Solaimani, R. H. Schiestl, *Cancer Res.* **2009**, *69*, 8784.
[13] K. Hirakawa, M. Mori, M. Yoshida, S. Oikawa, S. Kawanishi, *Free Radic. Res.* **2004**, *38*, 439.
[14] Y. L. Zhu, J. W. Eaton, C. Li, *PLoS One* **2012**, *7*, e50607.
[15] Y. Kubota, T. Shuin, C. Kawasaki, M. Hosaka, H. Kitamura, R. Cai, H. Sakai, K. Hashimoto, A. Fujishima, *Brit. J. Cancer* **1994**, *70*, 1107.
[16] M. Ethirajan, Y. H. Chen, P. Joshi, R. K. Pandey, *Chem. Soc. Rev.* **2011**, *40*, 340.
[17] R. Bonnett, *Chem. Soc. Rev.* **1995**, *24*, 19.
[18] R. R. Bacsa, J. Kiwi, *Appl. Catal. B-Environ.* **1998**, *16*, 19.
[19] T. Ohno, K. Sarukawa, K. Tokieda, M. Matsumura, *J. Catal.* **2001**, *203*, 82.
[20] T. Ashikaga, M. Wada, H. Kobayashi, M. Mori, Y. Katsumura, H. Fukui, S. Kato, M. Yamaguchi, T. Takamatsu, *Mutat. Res. Genet. Toxicol. Environ. Mutagen.* **2000**, *466*, 1.
[21] K. Nagaveni, G. Sivalingam, M. S. Hedge, G. Madras, *Appl. Catal. B Environ.* **2004**, *48*, 83.
[22] T. A. Konovalova, J. Lawrence, L. D. Kispert, *J. Photochem. Photobiol. A Chem.* **2004**, *162*, 1.
[23] K. Kamps, R. Leek, L. Luebke, R. Price, M. Nelson, S. Simonet, D. J. Eggert, T. A. Atesin, E. M. B. Brown, *Integr. Biol.* **2013**, *5*, 133.
[24] M. Kosmulski, *Adv. Colloid Interface Sci.* **2002**, *99*, 255.
[25] H. J. Nam, T. Amemiya, M. Murabayashi, K. Toh, *J. Phys. Chem. B* **2004**, *108*, 8254.

[26] S. J. Xiong, S. J. George, Z. X. Ji, S. J. Lin, H. Y. Yu, R. Damoiseaux, B. France, K. W. Ng, S. C. J. Loo, *Arch. Toxicol.* **2013**, *87*, 99.
[27] T. Rajh, M. C. Thurnauer, P. Thiyagarajan, D. M. Tiede, *J. Phys. Chem. B* **1999**, *103*, 2172.
[28] G. S. Li, L. P. Li, J. Boerio-Goates, B. F. Woodfield, *J. Am. Chem. Soc.* **2005**, *127*, 8659.
[29] C. C. Wang, J. Y. Ying, *Chem. Mat.* **1999**, *11*, 3113.
[30] B. L. Cushing, V. L. Kolesnichenko, C. J. O'Connor, *Chem. Rev.* **2004**, *104*, 3893.
[31] P. H. Mutin, A. Vioux, *Chem. Mat.* **2009**, *21*, 582.
[32] N. Pinna, M. Niederberger, *Angew. Chem. Int. Ed.* **2008**, *47*, 5292.
[33] I. Bilecka, M. Niederberger, *Electrochim. Acta* **2010**, *55*, 7717.
[34] R. Rossmanith, C. K. Weiss, J. Geserick, N. Husing, U. Hormann, U. Kaiser, K. Landfester, *Chem. Mat.* **2008**, *20*, 5768.
[35] M. Niederberger, *Accounts Chem. Res.* **2007**, *40*, 793.
[36] T. Kotsokechagia, F. Cellesi, A. Thomas, M. Niederberger, N. Tirelli, *Langmuir* **2008**, *24*, 6988.
[37] T. Kotsokechagia, N. M. Zaki, K. Syres, P. de Leonardis, A. Thomas, F. Cellesi, N. Tirelli, *Langmuir* **2012**, *28*, 11490.
[38] M. Niederberger, M. H. Bartl, G. D. Stucky, *Chem. Mat.* **2002**, *14*, 4364.
[39] B. Nair, *Int. J. Toxicol.* **2001**, *20*, 23.
[40] G. V. Jensen, M. Bremholm, N. Lock, G. R. Deen, T. R. Jensen, B. B. Iversen, M. Niederberger, J. S. Pedersen, H. Birkedal, *Chem. Mat.* **2010**, *22*, 6044.
[41] B. E. Yoldas, *J. Mater. Sci.* **1986**, *21*, 1087.
[42] G. Garnweitner, C. Grote, *Phys. Chem. Chem. Phys.* **2009**, *11*, 3767.
[43] M. Niederberger, G. Garnweitner, *Chem.-Eur. J.* **2006**, *12*, 7282.
[44] S. Schattauer, B. Reinhold, S. Albrecht, C. Fahrenson, M. Schubert, S. Janietz, D. Neher, *Colloid Polym. Sci.* **2012**, *290*, 1843.
[45] P. H. Wen, H. Itoh, W. P. Tang, Q. Feng, *Langmuir* **2007**, *23*, 11782.
[46] G. Colon, P. Sampedro, M. Fernandez-Garcia, H. Y. Chen, J. C. Hanson, J. A. Rodriguez, *Langmuir* **2008**, *24*, 11111.
[47] J. I. Langford, A. J. C. Wilson, *J. Appl. Crystallogr.* **1978**, *11*, 102.
[48] V. Uvarov, I. Popov, *Mater. Charact.* **2007**, *58*, 883.
[49] A. A. Gribb, J. F. Banfield, *Am. Miner.* **1997**, *82*, 717.
[50] Z. Y. Meng, S. M. Hashmi, M. Elimelech, *J. Colloid Interf. Sci.* **2013**, *392*, 27.
[51] A. V. Filippov, M. Zurita, D. E. Rosner, *J. Colloid Interf. Sci.* **2000**, *229*, 261.
[52] G. C. Bushell, Y. D. Yan, D. Woodfield, J. Raper, R. Amal, *Adv. Colloid Interface Sci.* **2002**, *95*, 1.
[53] H. Wu, M. Lattuada, P. Sandkuhler, J. Sefcik, M. Morbidelli, *Langmuir* **2003**, *19*, 10710.
[54] D. Wei, H. Wu, Z. B. Xia, D. L. Xie, L. Zhong, M. Morbidelli, *Colloid Polym. Sci.* **2012**, *290*, 1033.
[55] M. Rivallin, M. Benmami, A. Gaunand, A. Kanaev, *Chem. Phys. Lett.* **2004**, *398*, 157.
[56] T. D. Waite, A. I. Schafer, A. G. Fane, A. Heuer, *J. Colloid Interf. Sci.* **1999**, *212*, 264.
[57] M. Lattuada, P. Sandkuhler, H. Wu, J. Sefcik, M. Morbidelli, *Adv. Colloid Interface Sci.* **2003**, *103*, 33.
[58] R. Finsy, N. Dejaeger, R. Sneyers, E. Gelade, *Part. Part. Syst. Charact.* **1992**, *9*, 125.